PHYSICAL REVIEW D VOLUME 19, NUMBER 11 1 JUNE 1979

Inclusive charged-particle production in neutron-nucleus collisions

D. Chaney,* T. Ferbel, P. Slattery, and D. Underwood†
Department of Physics and Astronomy, University of Rochester, Rochester, New York 14627

E. Bleser‡ and D. Johnson
Fermi National Accelerator Laboratory, Batavia, Illinois 60510

B. Gobbi, R. Lipton, J. Rosen, R. Ruchti,§ and D. Spelbring
Department of Physics and Astronomy, Northwestern University, Evanston, Illinois 60201

(Received 2 January 1979)

We have measured charged-particle production in neutron-nucleus collisions at high energy. Data on positive and negative particles produced in nuclei [ranging in atomic number (A) from beryllium to lead] are presented for essentially the full forward hemisphere of the center-of-mass system. A rough pion-proton separation is achieved for the positive spectra. Fits of the form A^{α} to the cross sections are presented as functions of transverse momentum, longitudinal momentum, rapidity, and pseudorapidity. It is found that α changes from ~ 0.85 to ~ 0.60 for laboratory rapidities ranging from 4 to 8. Trends in the data differ markedly when examined in terms of pseudorapidity rather than rapidity. Qualitatively, the major features of our data can be understood in terms of current particle-production models.

INTRODUCTION

Our present knowledge of the strong interaction is based largely on studies of hadron-hadron scattering. In any such experiment we only measure the asymptotic states, and we therefore have very little insight into the nature of hadronic matter at the time of its creation. It is possible, however, to affect the early stages of an interaction and learn about hadronic matter at nascency by using nuclear targets. When a high-energy projectile collides with a nucleus and interacts with one of the nucleons, the remaining nucleons serve as secondary targets for the reinteraction of the states produced in the initial collision. By varying the atomic number of the targets, one can observe differences in production which should be attributable to the intimate details of the strong interaction over short space-time intervals. One of the simplest effects to study would be the change of the multiplicity (the number of particles produced per inelastic collision) with atomic weight (A). If the final-state hadrons in a hadron-nucleon interaction were completely formed within a distance of approximately the size of a nucleon, the individual products of the initial strong interaction could interact with the nucleons remaining downstream of the first point of collision, and produce a cascading effect, leading to a strong dependence of the multiplicity on A. If, on the other hand, particles produced in the initial collision required much time to separate and resolve into their final states, then the multiplicity would not depend radically on A. The latter situation could be realized, for example, in a primary interaction which produced a correlated or resonance like system of hadrons (acting as a single object as it traversed nuclear matter).

Early observations in cosmic-ray studies[1] have shown evidence for a lack of cascading in nuclei at high energies, and recent measurements at Fermilab[2] have confirmed these findings. In our experiment we provide detailed measurements of particle production in neutron-nuclear collisions, for essentially the full forward hemisphere of the center of mass, with information on charge, transverse momentum, and longitudinal momentum of hadrons.

Current models of particle production have had substantial success in treating the qualitative properties of hadron production in hadron-nucleus collisions. Multiperipheral models,[3] energy-cascade models,[4] parton models,[5] and other phenomenological ideas[6] have made similar predictions concerning the A dependence of the multiplicity. Our new data should provide a great challenge for these models and thereby point to those that are most likely to provide a greater insight into the strong interaction.

I. EXPERIMENTAL DETAILS

A. Beam, targets, and spectrometer

The experiment was performed in the M-3 beam line[7] at the Fermi National Accelerator Laboratory (Fermilab). The production angle for this neutral secondary beam was 1 mr relative to the incident primary 400-GeV proton beam. The target used to produce the secondary beams at the Meson Laboratory was a 20-cm-long bar of beryllium, 0.16

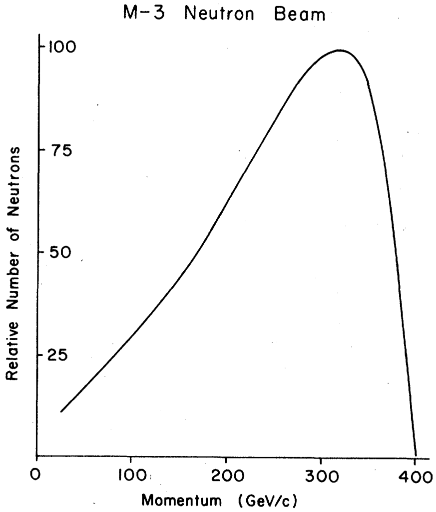

FIG. 1. Momentum spectrum of the neutron beam.

cm by 0.16 cm in size in the plane perpendicular to the beam.

The properties of the beam have been described elsewhere[8-10]; here we only provide the momentum spectrum of the neutron flux (Fig. 1).[9] During typical running conditions, there were 5×10^4 neutrons incident on the experimental target, during a beam-spill time which lasted 2 sec. The transverse size of the beam was about 1 mm×1 mm. Contamination from K_2^0, $\bar{n}$, and photons in the beam is estimated to be less than 1%, and concentrated mainly for momenta well below 100 GeV/c.

The University of Michigan provided their total-absorption calorimeter,[11] which we utilized for counting neutrons in the beam. The active area of the calorimeter corresponded to a 24-in.×24-in. square, perpendicular to and centered on the beam; the device was situated about 100 m downstream from our target. This calorimeter was the same one used in establishing the particle composition and spectrum of the neutral beam.[8,9]

Targets used in the experiment corresponded to approximately 1% to 5% absorption lengths of material (see Table I). In addition to obtaining data using five different nuclei, we also had runs using two different thicknesses of lead (as well as runs with no target in place) to gauge the effects of background and multiple scattering.

Elements of the spectrometer (shown in Fig. 2) were used to detect interactions in the nuclear targets, and to measure and record properties of charged particles produced in those interactions. Fast electronic-logic signals from scintillation counters (A, S, and L) were used to select appropriate events for triggering two modules of wire spark chambers (WSC1 and WSC2). The analysis magnet (BM109) imparted a 510-MeV/c transverse impulse to charged particles; the aperture was 8 in. vertically, 24 in. horizontally (bending plane), and 72 in. along the beam axis.

B. L counter and spark chambers

The L counter was a Teflon-coated liquid-scintillation counter, constructed of 0.125-in.-thick aluminum channel, with inner dimensions of 4.6 cm along the beam direction, 3.2 cm in the vertical, and 2.2 m in the horizontal direction (perpendicular to the beam). The channel was closed at both ends with transparent Lucite spacers which permitted the transmission of light from the liquid scintillator to photomultiplier tubes attached to the Lucite material. Signals from the photomultiplier tubes were used as part of the trigger, and were also recorded for use in the off-line analysis.

The L counter was located at the downstream end of the spectrometer, a little over 10 m from the target. Two strips of lead, each 0.75 in. thick, 1.75 in. high, and 45 in. long, were placed end to end with a 2-in.-wide separation between them, in front of the counter. This lead was used to generate electromagnetic cascades which could be detected in the L counter.

Two plastic scintillation counters, A and S, were placed in front of, and behind the target, respec-

TABLE I. Properties of the targets. l_{abs} is the nucleon absorption length for the material. l_{rad} is the radiation length for the material. Values of the parameters for the nuclei obtained from Particle Data Group, Rev. Mod. Phys. 48, S 1 (1976).

Element	Atomic weight (A)	Thickness (l) (cm)	Thickness (l) (g/cm^2)	l/l_{abs} (%)	l/l_{rad} (%)
Beryllium	9.01	2.078	3.84	5.66	5.91
Aluminum	26.98	1.798	4.85	4.83	20.2
Copper	63.54	0.645	5.78	4.36	45.1
Tin	118.7	0.632	4.62	2.77	52.2
Lead	207.2	0.318	3.61	1.72	56.8
Lead	207.2	0.170	1.93	0.919	30.4

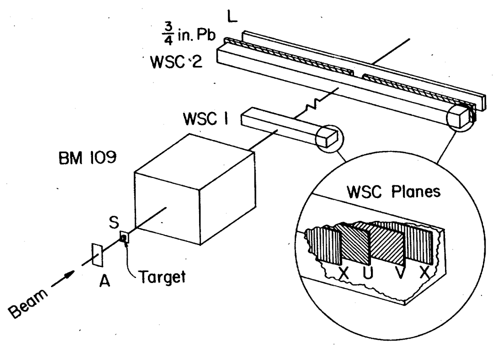

FIG. 2. Elements of the experimental spectrometer.

tively. Scintillator A was 0.125 in. thick, 4 in. high, and 4 in. wide; it was located about 9 in. in front of the target. The S counter was located immediately behind the target, and its active portion was a 0.25-in.-diameter disk that was approximately 0.0625 in. thick.

Charged particles were detected using two modules of magnetostrictive-readout wire spark chambers (WSC). Each module consisted of four gaps, and each gap was defined by a pair of 40 wire/in. parallel-wire planes. The wire planes were oriented perpendicular to the beam axis; two gaps in each module had vertical wires (X) while the other two gaps had wires inclined at ±15° to the vertical (U, V). The two modules were situated approximately 5 and 10 m downstream of the target. The spark-chamber module located closer to the magnet had a sensitive area 3 cm in the vertical dimension and 1 m in the horizontal; the downstream chamber's aperture was 5 cm by 2.3 m. The narrow-slit design provided for relatively simple track reconstruction.

C. The trigger and data taking

The basic idea of the trigger was simply to select those events which had a charged particle traversing the spark chambers. An event of interest was required to satisfy all of the following criteria:

(i) No charged particle was to be incident on the target (no signal in A).

(ii) At least one charged particle had to exit from the target (a signal in S).

(iii) At least one charged particle had to exit from the back of the spark chambers (a signal in L).

Consequently, the trigger requirements can be summarized as

$$\text{Trigger} = \bar{A} \cdot S \cdot L \,.$$

This trigger was very efficient in eliminating interactions initiated by charged particles; but it was less effective in ensuring that interactions originated in the target (as opposed to, for example, in the S counter), or that there were good tracks in the spark chambers. These problems will be addressed in the analysis section of this paper.

Every time an acceptable event was detected, the spark-chamber coordinates (obtained using time-to-digital converters), photomultiplier signals from sundry monitors and counters, and integrated pulse heights from the L counter were collected using a CAMAC system interfaced to and controlled by a DEC PDP-15 computer. The computer was programmed to monitor the performance of the experimental apparatus and to transfer the digital information for each event to a magnetic tape for subsequent off-line analysis.

The data were obtained during about three days of beam time. Approximately 130 000 triggers were collected during this time interval, with the data divided almost equally among the five target nuclei and target-empty running. Details concerning beam-monitoring procedures and the determination of the neutron flux can be found elsewhere.[10]

II. ANALYSIS AND CORRECTION OF DATA

Several sources of background were investigated and resultant corrections applied to the data. Using data accumulated with no target in place, we performed a background subtraction (ranging from ~8% for Be to ~28% for the thinner Pb sample) from data taken with nuclear targets in the beam. Also, various selection criteria were applied to the data to reduce backgrounds; these criteria are described below.

A. Electron contamination

Nonhadronic background in the data, due to the conversion of photons (mainly from π^0 mesons) into electrons and positrons, was reduced, on a statistical basis, with the aid of the pulse-height information from the L counter. This liquid scintillation counter, located at the downstream end of the spectrometer, was used both in the triggering and in electron identification. The vertical size of the counter was smaller than that of the active areas of the spark chambers, and consequently the counter set the limiting aperture for the spectrometer. Indeed, the region of acceptance for the L counter was well within the edges of the spark chambers, where track efficiency might have been poor.

Properties of the L counter, and its response to electrons that traversed the 0.75-in.-thick lead radiator, positioned 2 in. upstream of the counter, are detailed elsewhere.[10] In essence, the lead strips served as initiators of electromagnetic showers; such showers are characterized by a large charged-particle multiplicity and consequently by large pulse heights in the L counter.

Charged hadrons produced in the initial neutron-target interactions can, of course, interact inelastically in the downstream lead radiator and sometimes also yield large pulse-height signals in the L counter. To discriminate between true electron showers and hadronic interactions simulating such showers (we estimate that approximately 14% of the pions interacted in the lead and gave large signals in the L counter), we took advantage of the fact that the pion momentum spectrum cuts off essentially at ~100 GeV/c (see later), and consequently the contribution from electrons could only be important below 25 GeV/c. We eliminated from consideration as hadrons particles with momenta below 25 GeV/c if either (1) pulse heights from both ends of the L counter were above a predetermined minimum value,[10] or (2) the track in question passed through the gap in the lead radiator (i.e., no electron discrimination was available). Those tracks with momenta below 25 GeV/c that did *not* satisfy either (1) or (2) above were accepted as hadrons. Corrections were subsequently applied to the data to account for losses due to the cut at 25 GeV/c.

Using the above criteria to define electron candidates, the ratio of electrons to pions was estimated, separately for each target sample, and plotted (Fig. 3) as a function of target thickness, in units of radiation lengths of material (l/l_{rad}). If our criteria were valid, we would expect the extrapolation to $l=0$ (no target) to determine the fraction of hadrons that simulate electronlike signals in the L counter. (The target-empty result, which corresponds essentially to $l=0$, is shown with the other data points in Fig. 3.) The straight line in Fig. 3 is a least-squares fit to the data points (excluding the target-empty point); the fit yields the estimated e/π ratio of $(0.122\pm0.006)+(0.083\pm0.015)l/l_{\text{rad}}$. The extrapolation to $l=0$ is clearly consistent with the ratio from target-empty running, and also consistent with the ~14% estimate for the fraction of pions that we expect to interact in the radiator and be mistaken for electrons. Thus, we believe that the electron background in this experiment is understood at the level of statistical uncertainty of the data.

B. Proton sample

Assuming charge symmetry and factorization, the ratio of negative-pion to positive-pion production in the kinematic region of projectile fragmentation in neutron-nucleus collisions can be estimated to be about 3 : 1 (from results of experiments on inclusive pion production in pp reactions[12]). Thus we might naively expect far more negative-particle production than positive-particle production at large longitudinal momenta. However, the contribution from the fragmentation of neutrons into protons becomes substantial relative to the pion production at large momenta. In fact, it is expected that, at the very largest longitudinal momenta, the positively-charged-hadron spectrum will be dominated by protons. Since there is very little antiproton production expected, it would not be surprising if, instead of observing an excess of negative hadrons at large momenta, the opposite were true. (There are K^- and K^+ components in the hadron spectra, in addition to the p and $\bar{p}$ fractions; kaons, however, do not appear to dominate over pion production in any region of phase space.)

In Fig. 4 we plot the positive- and negative-hadron momentum spectra, for all targets, corrected only for geometric losses (see later). Positive particles are more copious than negative, and

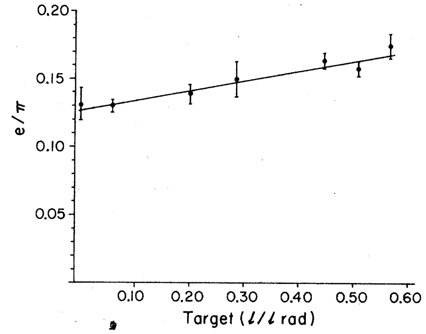

FIG. 3. Ratio of interpreted electrons to pions as a function of the number of radiation lengths of material present in the target. The straight line represents the best fit to the data points (excluding the target-empty point at $l=0$).

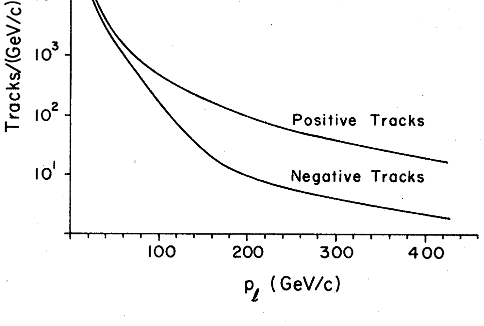

FIG. 4. Longitudinal-momentum distributions for reconstructed tracks, corrected for geometric losses.

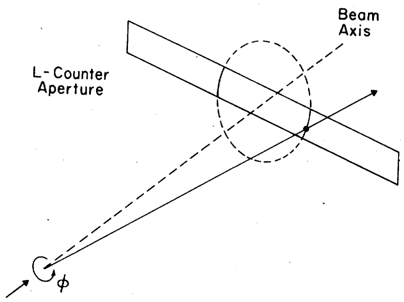

FIG. 5. Schematic of a track passing throught the L counter. The circle represents the family of intersection points when the track is rotated about the beam axis.

the difference is more pronounced at the largest momenta. Consequently, as indicated above, this result can be interpreted as being caused by the presence of protons in the data. Taking advantage of this, we defined a proton sample in the data as being comprised of positive tracks with momenta in excess of 80 GeV/c. Because some of the kinematic variables we will examine are affected by the mass interpretation given to the observed track (e.g., the rapidity), we will study the consequence of changing the mass interpretation when we present the data.

C. Event-weighting procedure

The geometrical arrangement of the apparatus and inefficiency in the operation of the spark chambers, naturally, precluded the detection of every produced charged particle. In fact, the spark chambers were specifically designed to have narrow apertures so as to avoid difficulties in reconstructing multiple tracks. Inefficiencies and losses in acceptance were compensated for by calculating the probability of observing any given event, and using the inverse of that probability as a weight for that event in determining production cross sections. The weighting procedures are described below.

1. Geometric losses

The active portion of each of the spark chambers was shaped in the form of a narrow slit and centered on the beam axis. On the average, 1–2 charged tracks per event traversed the chambers. Consequently, there was little ambiguity in correlating tracks from different views (X, U, and V coordinates) for spatial reconstruction of trajectories.

To correct for geometric loss of tracks that did not pass through the spark chambers, we proceeded as follows. Assuming that neither beam nor target were polarized (a very good approximation), the produced-particle spectrum could not have been a function of the azimuth angle (ϕ) about the beam axis. Therefore, any track observed within our (restricted) azimuthal acceptance represented a class of events with that particle's specific values of transverse momentum (p_T) and longitudinal momentum (p_l), and a uniform distribution in ϕ (including those values not in our acceptance). A typical track originating at the target and triggering the L counter is shown in Fig. 5. Its corresponding class of events would intersect the plane of the L counter on the indicated circumference of the sketched circle. The probability of detecting events of this particular class is defined by the ratio of the observed part of the circumference (the solid arcs) to the full circumference. The situation is actually somewhat more complicated than illustrated in the figure, because of the presence of the analyzing magnet. In reality, the charged tracks are bent within the magnet, and consequently the circle defining any particular class of events is displaced horizontally relative to the beam axis. The amount of this displacement is related to the values of p_T and p_l for that particular class of tracks. If the displacement is large enough, produced tracks of that class of events can be observed on only one side of the beam center and not on the other (true for particles having small momenta and therefore large bends in the magnet). These events pose no difficulty, except that they have two times larger weights.

There were, of course, classes of tracks that

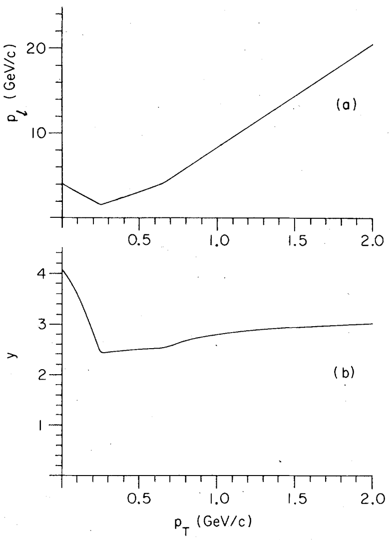

FIG. 6. Minimum values of longitudinal momentum (a) and rapidity (b) for which tracks are accepted in the spectrometer, as a function of transverse momentum. A pion mass was assumed in the calculations for (b).

were outside of the limits of our acceptance; these corresponded to particles produced at large angles or at very low momenta. Such events were lost and, clearly, could not be corrected for. In Fig. 6 we show the limits of the acceptance of the apparatus in p_l and y as functions of p_T. (The rapidity is defined as

$$y=\tfrac{1}{2}\ln[(E+p_l)/(E-p_l)]\,,$$

where E is the energy of the particle and p_l is its longitudinal momentum.) The two curves in the figure represent, for each value of p_T, the minimum values of p_l and y for tracks within the acceptance of the apparatus (i.e., tracks with values above either curve are accepted). We see that for a typical incident momentum of 300 GeV/c, our acceptance encompasses essentially the full range of the forward part of the center of mass. (A pion at rest in the center of mass has a value of $y=3.23$ for an incident momentum of 300 GeV/c.)

2. *Reconstruction efficiency of the spectrometer*

Tracks were reconstructed using sets of either three or four collinear sparks found in the four X (horizontal) wire planes; at least three collinear points in Y (vertical), obtained from the rotated U and V planes (matched with the line found in the X planes), were also required to consider any track acceptable. The collinearity requirement allowed ±1-mm spark deviations from a straight line in the X planes (±3 mm for V and U). The resulting distribution of sparks around the fitted tracks had a half width at half maximum of about 0.2 mm (0.8 mm for the rotated planes).

We determined the efficiency of the spectrometer by taking advantage of the expected azimuthal symmetry of particle production about the beam direction (or Z axis). Referring to Fig. 5, the circle of rotation traced by the intersection of the track with the plane of the L counter has two arcs which are within the acceptance of the spectrometer. Except for statistical fluctuations, the number of produced tracks, of any specific configuration of p_T, p_l, and charge, must be the same for both arcs. Thus, comparing the numbers of tracks actually observed provides an estimate of the spectrometer's relative track detection efficiency in the regions of the two arcs. Because the radius of the circle of rotation depends on the polar production angle ($\tan\theta=p_T/p_l$), and because the position of the center of the circle varies with the momentum of the particle (the bend of the trajectory in the magnet is, for simplicity, not shown in Fig. 5), relative detection efficiencies can, in fact, be obtained for any two arbitrary points along the L counter. Average efficiencies as a function of X were determined from these two-point comparisons, as described below.

Defining $N=110$ intervals of position along the L counter (X), we formed a two-dimensional array A_{ij} of the number of observed tracks which traversed the ith interval along the L counter and which would have traversed the jth interval if the production vector were rotated 180° in azimuth. (Tracks having p_T and p_l combination which, when rotated, fell outside the acceptance were not used in this analysis.) Defining ϵ_i as the inverse of the efficiency for tracks in the ith interval (i.e., n_i/ϵ_i of the n_i tracks were *observed* to traverse the ith interval of the L counter), we set up the following system of N linear equations in N unknowns, equating the sum of all tracks which intersected the ith interval to the sum of all tracks which could intersect the ith interval, upon an azimuthal rotation of 180°:

$$\sum_{j=1}^{N} A_{ji}\epsilon_j=\sum_{j=1}^{N} A_{ij}\epsilon_i=\epsilon_i\sum_{j=1}^{N} A_{ij}\quad(i=1,N)\,.$$

Because the overall normalization cannot be obtained from just relative efficiencies, the above corresponds to only $N-1$ independent equations. We solved the set of equations for the ϵ_i and smoothed the results to minimize effects of statistical fluctuations between neighboring bins.

The absolute normalization of the ϵ_i was fixed using a second independent spectrometer, which consisted of large-acceptance wire spark chambers placed in front of, between, and behind the narrow chambers.[13] Only a small sample of events were reconstructed using both spectrometers, consequently, the acceptance was determined to adequate statistical accuracy only in the central region of the spectrometers; this, however, was sufficient to fix the overall normalization of the efficiencies for the narrow chambers. Through examining

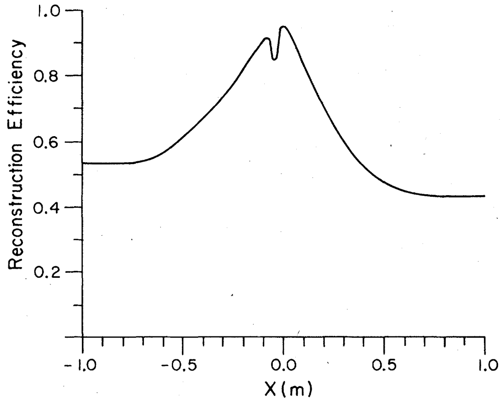

FIG. 7. Overall reconstruction efficiency as a function of position at the L counter, as determined by a comparison of symmetrically produced tracks.

tracks found in the large spectrometer, we found that the upstream module of narrow spark chambers was uniformly efficient across its entire aperture, and that the efficiency of the downstream module did not vary in the vertical dimension. This confirmed that our characterization of the spectrometer efficiency by a function of a single variable, namely X, was adequate.

The overall results of the efficiency analysis are shown in Fig. 7. The relative accuracy of the fitted values ranges from 10% near the edges of the chamber and in the central dip region to about 3% just outside the central dip. The somewhat unusual shape of the efficiency function (discussed more extensively in Ref. 10) can be accounted for on the basis of the structural characteristics of the two modules of spark chambers.

3. Overall acceptance

The two preceding subsections dealt with the event-weighting criteria. In addition to correcting data for geometric and reconstruction efficiency, we imposed several cuts on the data which we also took into account in the extraction of cross sections. The electron cuts we imposed required that we eliminate from the data sample those tracks with $p_l < 25$ GeV/c which either traversed the gap in the lead radiator or produced a large signal in the L counter. To correct for the loss of hadrons resulting from the imposition of these criteria, the weights for accepted tracks with $p_l \leq 25$ GeV/c were increased by a multiplicative factor of 1.12 (see Fig. 3); finally, when an azimuthally rotated track fell in the gap between the lead radiators, the weight for the track was increased by a factor of 2.

In Fig. 8 we display the average efficiency assigned to tracks, plotted as a function of p_T, p_l, and y. Part (a) shows the efficiency versus transverse momentum for four regions of longitudinal momentum. The dips near $p_T \simeq 0.4$ GeV/c arise from the exclusion of tracks (with momenta below 25 GeV/c) that traverse the gap in the lead radiator. Part (b) of the figure displays the average efficiency plotted against p_l for four regions in p_T. In part (c) we show the efficiency as a function of laboratory rapidity. The rapidity is closely related to pseudorapidity variable η, which is defined in terms of the polar production angle θ in the laboratory as

$$\eta = -\ln[\tan(\theta/2)] \approx y .$$

The miniscule efficiency at small rapidity arises from the fact that these tracks are produced, typically, at large angles and hence are not readily detected in the apparatus.

III. RESULTS OF THE EXPERIMENT

We will present the results of our experiment in the form of multiplicity distributions. The multiplicity is defined as the observed cross section for the process under consideration divided by the total inelastic cross section (i.e., the average number of times that a specified result occurs per collision). We use the following approximate expression for the total inelastic cross sections[15]:

$$\sigma^{A}_{\mathrm{INEL}} = 46A^{0.69}\ \mathrm{mb} ,$$

where A is the gram-atomic weight of the nuclear target. We extracted the A dependence for any region of phase space by fitting the five nuclear cross sections to a function of the form const$\times A^{\alpha}$. A value of $\alpha = 0.69$ would imply that the multiplicity is independent of nuclear size, or that the nucleus is trasparent to the hadronic system produced in the initial collision; this is something which would not be expected for hadronic reactions.

In the following sections we examine the dependence of the data on transverse momentum (p_T), laboratory rapidity (y), pseudorapidity (η), long-

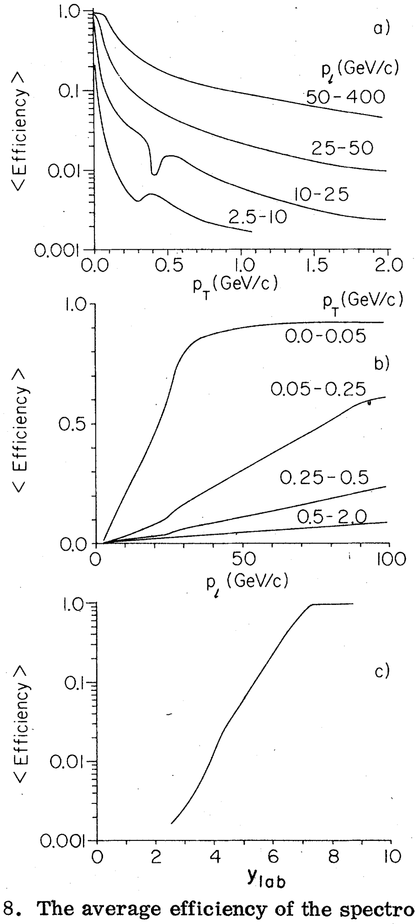

FIG. 8. The average efficiency of the spectrometer, shown as a function of several variables of interest.

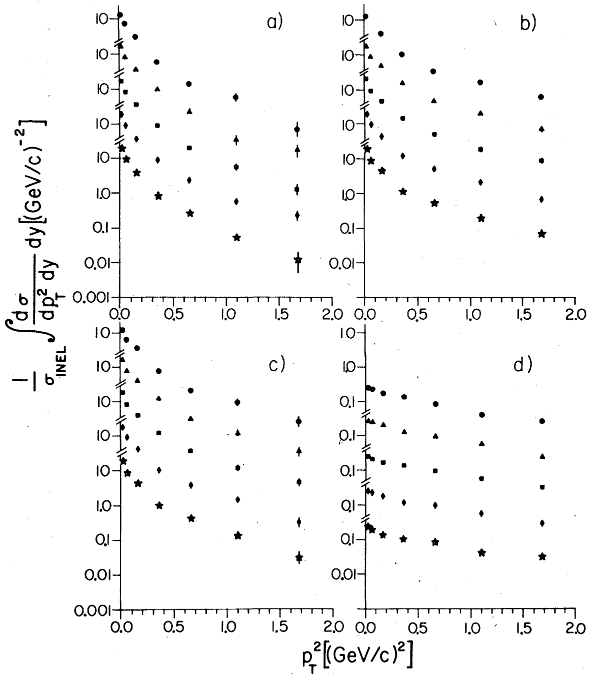

FIG. 9. Multiplicity as a function of the square of the transverse momentum, for rapidities greater than 4. (a) All negative particles (b) all positive particles (c) positive "pions" (longitudinal momentum less than 80 GeV/c) (d) "protons" ($p_l > 80$ GeV/c). In each graph, the five types of nuclear targets are denoted by the following symbols: Be:●, Al:▲, Cu:■, Sn:◆, Pb:★.

itudinal momentum (p_l), and combinations of these variables. Statistical errors will be included in the figures, and possible systematic biases will be discussed later in this section.

A. Dependence on transverse momentum

In Fig. 9 we show the produced-particle multiplicity, integrated for $y > 4$, as a function of p_T^2 for each of the target nuclei. The positive particles are examined in three ways: First, all the data are given without differentiation according to longitudinal momentum, and then the positives are separated into "pions" and "protons" using our division at $p_l = 80$ GeV/c (tracks with longitudinal momenta above this value are interpreted as protons). The pion distributions are all steeply falling for $p_T^2 \leq 0.3$ (GeV/c)^2, beyond which the p_T dependence is more akin to that observed for the proton data. Although the p_T^2 distributions for all particles become less steep with increasing longitudinal momentum, the positive spectra exhibit a substantially weaker p_T^2 dependence than the negative-particle spectra. We attribute this difference partially to the presence of the proton component in the data. The difference is particularly pronounced at larger p_T^2 where the remnant proton component, even for $p_l < 80$ GeV/c, may be substantial.

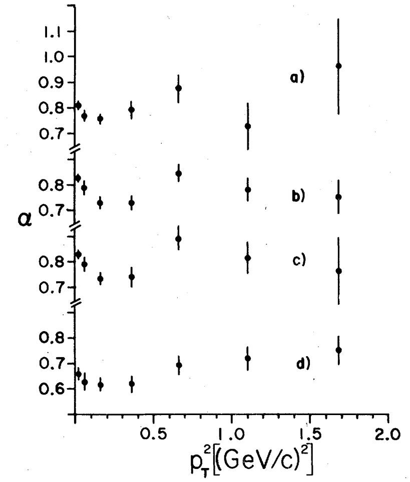

FIG. 10. Atomic-weight dependence of the cross sections as a function of the square of the transverse momentum, for rapidities greater than 4. (a) All negative particles (b) all positive particles (c) positive "pions" (d) "protons."

The dependence of the p_T^2 distributions on nuclear size is shown in Fig. 10, where we plot α as a function of p_T^2, for the data illustrated in the previous figure. The graph for negative particles shows a peak for α at small p_T^2, followed by a falloff and a constant region at larger values of p_T^2. The graph for positive particles shows similar behavior; when we split these data into "pion" and "proton" components, we see that the small-p_T^2 peak appears to be caused by the pions. The numerical values of the data points used in Figs. 9 and 10 are given elsewhere.[16]

B. Dependence on longitudinal momentum and rapidity

The atomic-weight dependence of the data on longitudinal momentum is displayed in Fig. 11.

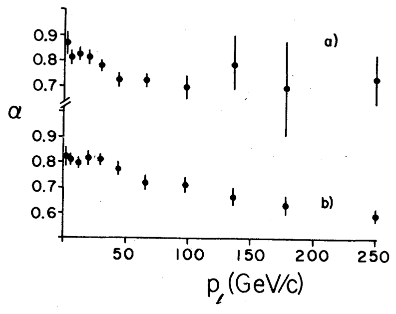

FIG. 11. Atomic-weight dependence of the cross section as a function of longitudinal momentum. (a) All negative particles (b) all positive particles.

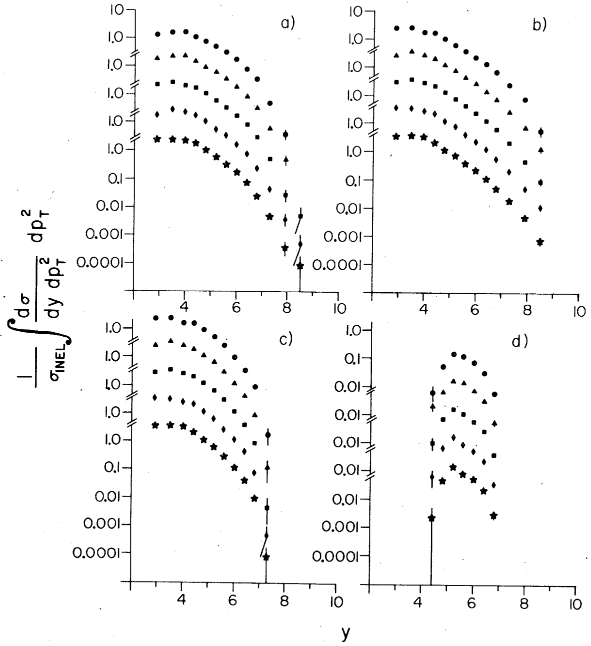

FIG. 12. Multiplicity as a function of rapidity. (a) All negative particles (b) all positive particles (pion mass assumed) (c) positive "pions" (d) "protons". In each graph, the five types of nuclear targets are denoted by the following symbols: Be: ●; Al: ▲; Cu: ■; Sn: ◆; Pb: ★.

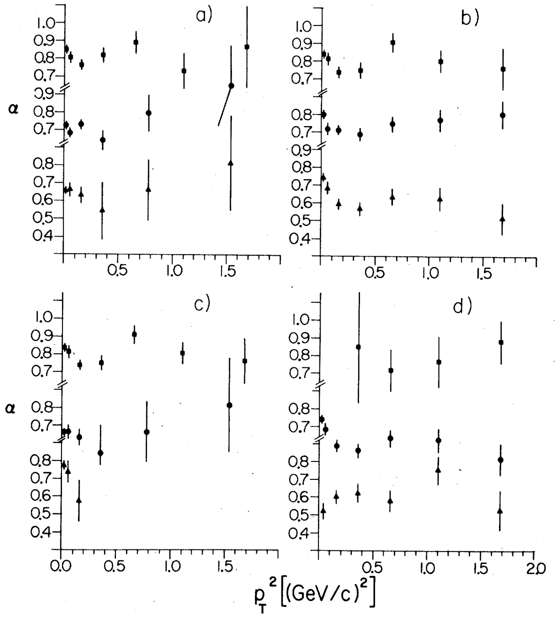

FIG 14. Atomic-weight dependence of the cross section as function of the square of the transverse momentum for different regions of rapidity. ■: 4 $<y<5$; ●: 5 $<y<6$; ▲: 6 $<y<8$. (a) All negative particles (assuming pion mass) (c) positive "pions" (d) "protons".

The data have been integrated over p_T, and the noninvariant cross sections $(d\sigma/dp_t)$ fitted to the form A^α. There appears to be a significant A dependence in the data, particularly at small values of p_t. The positive and negative data are very much the same; even at large p_t values, where protons dominate the positive-particle data, we do not observe any statistically significant difference. The numerical values of α, and of the produced multiplicity for the individual nuclear targets, as functions of p_t, can be found elsewhere.[16]

In Fig. 12 we display the multiplicity, integrated

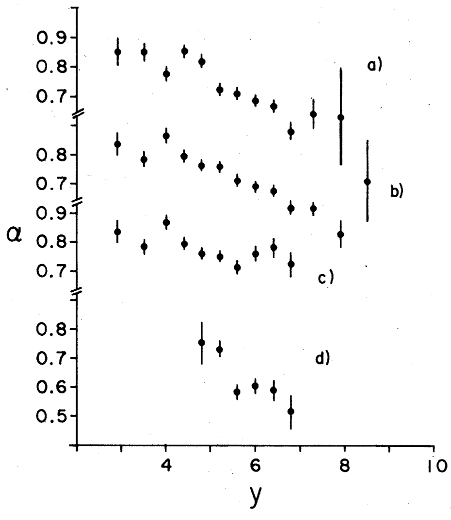

FIG. 13. Atomic-weight dependence of the cross section as a function of rapidity. (a) All negative particles (b) all positive particles (pion mass assumed) (c) positive "pions" (d) "protons".

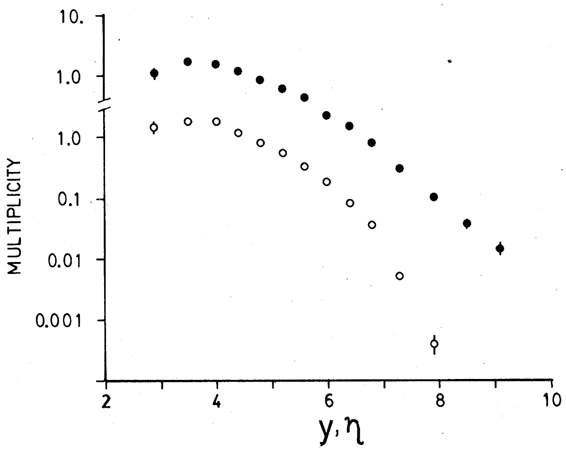

FIG. 15. Comparison between rapidity (○) and pseudorapidity (●). Multiplicity as a function of the two variables, plotted on the same axis, for negative particles from a beryllium target.

over p_T^2, as a function of rapidity (y) for all the targets; the positive spectra [shown in part (b), assuming a pion mass] are again divided into "pions" and "protons" in parts (c) and (d), respectively. (To avoid confusion, the data for each target were shifted by a decade relative to the previous sample. The data are displayed from top to bottom in order of increasing A.) Below $y \simeq 4$ our acceptance deteriorates and, consequently, the *absolute* normalization there is not reliable. (The error bars in the figure, as mentioned previously, are only statistical.) The atomic-weight dependence of the distributions in Fig. 12 is shown in Fig. 13, where we plot α as a function of rapidity. For both positive particles and negative particles, α decreases with increasing y, falling below 0.69 for $y \gtrsim 6$. For "protons" (the rapidity calculated using a proton mass), α decreases to ~0.5 at large y. The values of the data points depicted in Figs. 12 and 13 are tabulated in Ref. 16.

C. Correlations between y and p_T

We now proceed to a more detailed examination of the A dependence of the data. In Fig. 14 we show the p_T^2 dependence of the α parameter for three different regions of rapidity (calculated using the *pion* mass): $4<y<5$, $5<y<6$, $6<y<8$. The variation of α with p_T^2 appears to depend on y. In particular, negative particles exhibit a clear peak in the α distribution at small p_T^2 only for the lowest region of rapidity. Positive particles, on the other hand, exhibit an increase in α at small p_T^2 for all y. Although this effect appears to be caused mainly by "pions," there is some indication of a similar tendency in the proton data; nevertheless, our crude pion-proton separation prevents us from reaching any definitive conclusions. Table V of Ref. 16 lists the values of α plotted in Fig. 14, along with the associated values of the multiplicities from the different targets. [Multiplicities and the fitted values of α as functions of p_T^2 (for $y>4$), separated into regions of longitudinal momentum, are tabulated elsewhere.[16]]

D. Comparison of dependence on rapidity and on pseudorapidity

The difference between rapidity (y) and pseudorapidity (η) is not large in most regions of phase space, and so the two are usually used interchangeably. At very small angles, however, the differences can be substantial.

The definition of rapidity, as measured in the laboratory frame of reference can be written as

$$y = -\ln[\tan(\psi/2)]\,,$$

where ψ is an angle defined by $\tan\psi = m_T/p_l$, and $m_T = (p_T^2 + m^2)^{1/2}$ is the "transverse" mass of a particle of mass m. The production angle of the particle in the laboratory frame θ enters into the analogous definition of η, with $\tan\theta = p_T/p_l$. The two angles ψ and θ in these definitions are approximately the same only at large p_T, that is, where the mass of the produced particle can be ignored relative to its transverse momentum.

In Fig. 15 we compare y and η distributions for negative tracks produced on a beryllium target (the two sets of data are shifted relative to each other by a decade). The multiplicity at regions of large rapidity is smaller than that at large values of η. This difference arises because different regions of phase space are examined for the same numerical value of y and η. Detailed comparison of the kinematics reveals, as might be expected, that the difference between the two variables is most pronounced at small p_T.[10]

The atomic-weight dependence as a function of pseudorapidity is shown in Fig. 16. (Figure 13 displays the dependence on rapidity.) A marked difference in the value of the α parameter is apparent at large values of the two variables. In both cases, initially α falls off as y and η increase; but α does not become as small, when examined as a function of η, as it did versus y. For $\eta>7$ (beyond the kinematic upper limit for y) the extracted values of α rise above the minimum value of ~0.7. To explore this effect further, in Fig. 17 we show the α parameter as a function of y and η, but with the data divided into different regions of p_l. The rise in α at large η is observed for all p_l; it is most pronounced, however, for both positive and negative tracks, in the $20<p_l<60$ GeV/c, where we have best statistics at large values of η. The data at large y have poor statistics, and we consequently cannot, with assurance, address the question of a rise in α for large y; there does, however, appear to be a small effect in the positive-particle data. (Tables for values of the multiplicities and of the α parameters, used in the above y-η comparison, are available in Ref. 16.)

E. Systematic errors

Cross sections (or multiplicities) reported in this paper have several sources of possible systematic uncertainty. Systematic biases stem from the uncertainty in the measurement of the neutron flux, from variations in the thickness of the nuclear targets, from residual contamination of the data (by electrons, kaons, stray tracks, etc.), from the idealized treatment of the apparatus in correcting for geometric losses, and from uncertainties in the determination of the efficiency of the spectrometer. (No corrections were applied for secondary interactions within the targets because

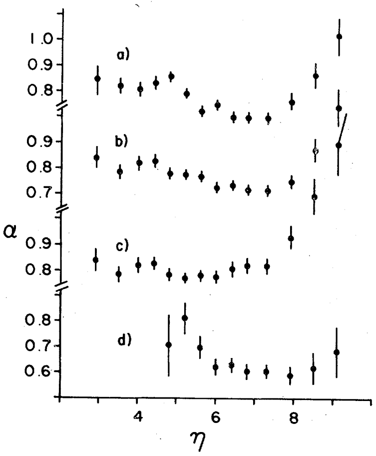

FIG. 16. Atomic-weight dependence as a function of pseudorapidity. (a) All negative particles (b) all positive particles (c) positive "pions" (d) "protons".

the effect is expected to be below the 5% level.) We estimate that the systematic biases contribute to a ±15% overall uncertainty in the absolute cross-sectional measurements. The neutron-flux normalization is the largest component of these biases, and crude cross checking leads us to believe that the error in the flux measurement is less than ~10%.[10] Possible electron contamination, which we expect to be localized to transverse momenta below $p_T^2 = 0.01$ (GeV/c)^2, is such that in this region of phase space we estimate that the remnant contamination justifies doubling of the presented statistical error bars, both for cross sections and for the α parameters. The systematic uncertainty in the determination of the atomic-weight dependence of the data (i.e., the α parameter) is difficult to assess. As can be observed from some of the poor χ^2 values for fits[16] of cross sections to the form A^α, this parametrization is not always appropriate. In fact, there are regions of phase space where more complicated functions are clearly required. It is for this reason that we would urge phenomenologists to use the tabulated cross sections,[16] rather than values of α for any detailed comparisons of our data with models.

Finally, we stress that because we cannot correct for data that are totally outside of the acceptance of our apparatus, the absolute values for differential cross sections in regions of marginal acceptance (<1%) must be viewed with great caution. Nevertheless, the A dependence of the data, even in regions of poor acceptance, should still be reliable.

F. Conclusions

There has recently been a renewal of interest in the study of particle production using nuclear targets.

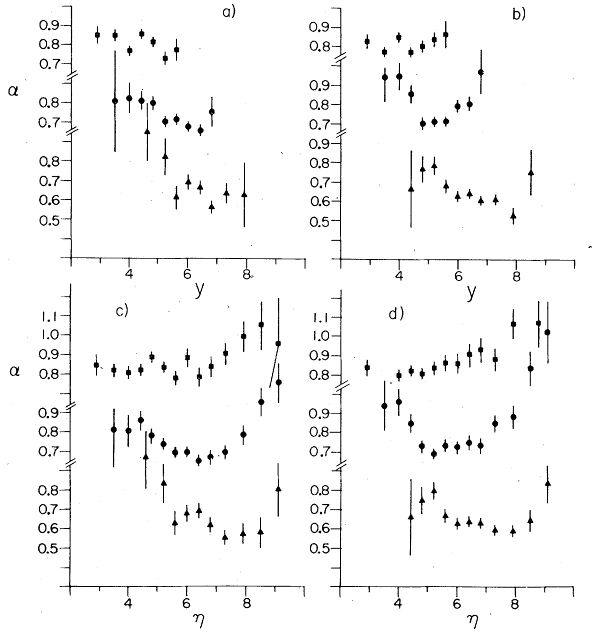

FIG. 17. Atomic-weight dependence as a function of rapidity and pseudorapidity for intervals of longitudinal momentum. ■: $2.5 < p_l < 20$ GeV/c; ●: $20 < p_l < 60$; ▲: $60 < p_l < 400$. (a) All negative particles versus rapidity (b) all positive particles versus rapidity (c) all negative particles versus pseudorapidity (d) all positive particles versus pseudorapidity.

Experiments performed in the past few years have reported features which agree qualitatively with those observed in our data. However, our experiment is unique in that we have measured momenta and angles of final-state particles for a variety of nuclear targets. Although a rise in α was observed previously[17] at small p_T^2 for a fixed production angle, our data have provided the evidence needed to show that this effect was not just a kinematic consequence of the fixed angle in that experiment (as was suggested by Dar *et al.*[18]), but a general phenomenon occurring over an extended region of phase space. The behavior of our data at large p_T^2 supports the small rise in α seen in previous proton-nucleus experiments.[19]

The atomic-weight dependence of the inclusive cross section as a function of pseudorapidity η has been investigated previously by others[20] and their results indicated that at small angles multiplicity becomes independent of A. Our data show a definite dependence on A, in that α falls well below a value of 0.69 at large rapidity. This observation excludes from consideration recently favored simple multiperipheral (single-Regge-pole exchange) and energy-flux-cascade models, and suggests that multi-Regge-pole exchanges or cut contributions are important in hadron-nucleus collisions.[3] However, when our data are examined as a function of η, the results are consistent with a lack of dependence of particle production on A for moderately large η $(5 < \eta < 7)$.[21] Consequently, it appears that theoretical predictions for $\alpha(y)$ cannot be assumed to hold without modification for $\alpha(\eta)$. While the decrease of α with increasing η (or y) can be explained by several diverse models,[22] the parton-cascade model[23] has explicitly predicted a decrease in α followed by a small increase at largest values of η. We, of course, observe a very large increase in α for $\eta > 7$. This rise in our data, however, might be caused, at least partially, by the electromagnetic interaction of the neutron producing a low-mass resonance [e.g., the $\Delta^0(1232)$] in the forward direction[24]; the nuclear dependence of such a reaction would be proportional to Z^2, and the coherent production cross section is large enough so that the decay products $(\Delta^0 \rightarrow p\pi^-)$ could provide a non-negligible contribution at small angles. At present, there is no clear understanding of the observed increase of α at small p_T,[25] nor do we believe that the increase of α for large η can be attributed entirely to Coulombic processes.[10] As for the rest of our findings, they appear to be in at least qualitative agreement with the predictions of a variety of models. Detailed calculations will be required to establish which of these models, if any, can provide an understanding of all of the production phenomena found in this work.

ACKNOWLEDGMENTS

We thank Dr. C. Brown, Dr. A. Greene, and the Fermilab staff for their support of the experiment that provided the source of the present data. We also thank A. Białas and M. Longo for comments on our manuscript. This research was supported in part by the U. S. Department of Energy.

---

*Present address: Bell Laboratories, Naperville, Ill. 60540.

†Present address: Argonne National Laboratory, Argonne, Ill. 60439.

‡Present address: Brookhaven National Laboratory, Upton, N.Y, 11973.

§Present address: Notre Dame University, Notre Dame, Ind. 46556.

[1] A. Gurtu *et al.*, in *Proceedings of the Fifth International Symposium on Many-Particle Hadrodynamics, Leipzig, 1974,* edited by G. Ranft and J. Ranft (Karl Marx Univ., Leipzig, German Democratic Republic, 1974), pp. 493–513.

[2] J. E. Elias *et al.*, Phys. Rev. Lett. 41, 285 (1978), and references given therein to previous work done by this group.

[3] J. Koplik and A. H. Mueller, Phys. Rev. D 12, 3638 (1975); A. Capella and Krzywicki, Phys. Lett. 67B, 84 (1977).

[4] K. Gottfried, Phys. Rev. Lett. 32, 957 (1974).

[5] S. J. Brodsky *et al.*, Phys. Rev. Lett. 39, 1120 (1977). For an approach based on constituent quarks see A. Białas *et al.*, Acta Phys. Pol. B8, 585 (1977), and A. Białas and W. Czyz, Cracow Report No. INP-1027/PH, 1978 (unpublished); also see A. Białas, Fermilab Report No. PUB 78/75 THY, 1978 (unpublished) for other references.

[6] G. Berlad, A. Dar, and G. Eilam, Phys. Rev. D 13, 161 (1976); A. Dar, talk given at the Topical Meeting on Multiparticle Production at Very High Energy, ICTP, Trieste, 1976 (unpublished).

[7] The data were taken as part of the background studies for an experiment searching for charmed particles at Fermilab (E397). For details see D. Spelbring *et al.*, Phys. Rev. Lett. 40, 605 (1978), and R. Lipton *et al.*, *ibid.* 40, 608 (1978).

[8] M. J. Longo *et al.*, University of Michigan Report No. UM HE 74-18 (unpublished). This report concerns conditions that obtained for 300-GeV/c primary protons.

[9] Results from the University of Michigan group, privately communicated to us by H. R. Gustafson, regarding conditions using 400-GeV primary protons. We estimate that the γ and K_L^0 components of the M-3 beam for 400-GeV incident protons are similar to those for 300 GeV (Ref. 8).

[10] D. Chaney, Ph.D. thesis, University of Rochester Report UR-679, 1978 (unpublished).

[11] L. W. Jones *et al.*, Nucl. Instrum. Methods 118, 431 (1974).

[12] R. Schindler *et al.*, Phys. Rev. Lett. 33, 862 (1974).

[13] The main spectrometer is described in D. Spelbring *et al.* (Ref. 7).

[14] Preliminary findings were reported in D. Chaney *et al.*, Phys. Rev. Lett. 40, 71 (1978).

[15] W. Busza, Acta Phys. Pol. B8, 333 (1977).

[16] D. Chaney *et al.*, University of Rochester Report No. UR-689, 1979 (unpublished).

[17] D. Garbutt *et al.*, Phys. Lett. 67B, 355 (1977).

[18] Private communication.

[19] J. W. Cronin *et al.*, Phys. Rev. D 11, 3105 (1975), and also Ref. 16.

[20] See, for example, the review of C. Halliwell, in *Proceedings of the VIII International Symposium on Multiparticle Dynamics, Kayersberg, 1977,* edited by R. Arnold *et al.* (Centre de Recherches Nucleaires, Strasbourg, France, 1977).

[21] See Ref. 19, and the more recent measurements of production in neutron-nucleus collisions by D. Burke *et al.*, Phys. Rev. D 19, 1616 (1979).

[22] The predictions of the coherent tube model are in good agreement with our data (private communication from A. Dar *et al.*). See also Refs. 3, 5, and 6.

[23] N. N. Nikolaev, predictions in S. A. Azimov *et al.*, paper submitted to the VII International Conference on High Energy Physics and Nuclear Structure, Zurich, 1977 (unpublished).

[24] A similar effect for proton production in neutron-nucleus collisions has recently been reported by M. R. Whalley *et al.*, University of Michigan Report No. UMHE 78-46 (unpublished).

[25] See, however, the remarks of J. Kühn, Phys. Rev. D 18, 338 (1978).